Projected near-term changes of temperature extremes in Europe and China under different aerosol emissions

Article

Published Version

Creative Commons: Attribution 4.0 (CC-BY)

Open Access

www.reading.ac.uk/centaur

LETTER • OPEN ACCESS

Projected near-term changes of temperature extremes in Europe and China under different aerosol emissions

To cite this article: Feifei Luo *et al* 2020 *Environ. Res. Lett.* **15** 034013

View the article online for updates and enhancements.

Environmental Research Letters

LETTER

Projected near-term changes of temperature extremes in Europe and China under different aerosol emissions

Feifei Luo[1,8] , Laura Wilcox[2], Buwen Dong[2] , Qin Su[3] , Wei Chen[4] , Nick Dunstone[5], Shuanglin Li[1,6] and Yongqi Gao[1,7]

[1] Nansen-Zhu International Research Centre and Climate Change Research Center, Institute of Atmospheric Physics, Chinese Academy of Sciences, Beijing, People's Republic of China
[2] National Centre for Atmospheric Science, Department of Meteorology, University of Reading, Reading, United Kingdom
[3] Department of Atmospheric Sciences, Yunnan University, Kunming, People's Republic of China
[4] State Key Laboratory of Numerical Modeling for Atmospheric Sciences and Geophysical Fluid Dynamics, Institute of Atmospheric Physics, Chinese Academy of Sciences, Beijing, People's Republic of China
[5] Met Office Hadley Centre, Exeter, United Kingdom
[6] Department of Atmospheric Science, China University of Geoscience, Wuhan, People's Republic of China
[7] Nansen Environmental and Remote Sensing Center and Bjerknes Centre for Climate Research, Bergen, Norway
[8] Author to whom any correspondence should be addressed.

E-mail: luofeifei212@mail.iap.ac.cn

Keywords: temperature extremes, anthropogenic aerosols, projection, HadGEM3-GC2

Supplementary material for this article is available online

Abstract

This study assesses near-term future changes in temperature extremes over China and Europe in scenarios with two very different anthropogenic aerosol (AA) pathways from 2016 to 2049: a maximum technically feasible aerosol reduction (MTFR), and a current legislation aerosol scenario (CLE), both with greenhouses gas forcing following RCP 4.5. Simulations with a fully coupled atmosphere-ocean model HadGEM3-GC2 show that there is an increase in hot extremes and a decrease in cold extremes relative to the present day (1995–2014) over China and Europe in both scenarios. However, the magnitude of the changes in both hot and cold extremes depends strongly on the AA pathway. The AA reduction in MTFR amplifies the changes in temperature extremes relative to CLE, and accounts for 40% and 30% of the projected changes in temperature extremes relative to present day over China and Europe, respectively. Thus, this study suggests that future and current policy decisions about AA emissions have the potential for a large near-term impact on temperature extremes.

1. Introduction

Alongside global warming, the intensity and frequency of temperature extremes have changed since the pre-industrial period, resulting in more hot extremes and fewer cold extremes in many regions (e.g. Alexander *et al* 2006, Donat *et al* 2013). Because temperature extremes often cause substantial economic and human losses, understanding the underlying drivers of changes in temperature extremes, and these changes in future, are of particular concern for both the scientific community and policy makers as they deal with climate changes and their impacts.

Anthropogenic forcing, including greenhouse gas (GHG) and anthropogenic aerosols (AA), has been shown to play a dominant role in observed changes in temperature extremes over different regions (Sun *et al* 2014, Fischer and Knutti 2015, Dong *et al* 2016a, 2016b, Chen and Dong 2018, Wilcox *et al* 2018). Many studies have therefore evaluated changes in future temperature extremes under different emission scenarios (Sillmann *et al* 2013a, Xu *et al* 2013, Wuebbles *et al* 2014, Zhou *et al* 2014, Xu *et al* 2018). In general, hot extremes will increase while cold extremes will decrease in magnitude and frequency with the warming trend in future, which is mainly attributed to increases in GHG concentrations (e.g. Tebaldi *et al* 2006, Sillmann *et al* 2013a). AA emissions are expected to decline in future, as a result of governments' efforts to improve air quality. Hence, a number of studies have investigated the changes in

temperature extremes under future scenarios of AA emission reductions, and suggested that the reduction of AA could greatly enhance the effect of GHG forcing (Mickley *et al* 2012, Sillmann *et al* 2013b, Wang *et al* 2016, Acosta Navarro *et al* 2017, Samset *et al* 2018, Hienola *et al* 2018). However, there is still a large uncertainty in the quantification of the effect of AA reduction, due to large uncertainties in models and scenarios.

In this study, we investigate changes in Chinese and European temperature extremes under a maximum technically feasible aerosol reduction (MTFR) scenario and a current legislation (CLE) scenario using the ECLIPSE (Evaluating the Climate and Air Quality Impacts of Short-lived Pollutants) V5a global emission fields with a fully coupled climate model. For the CLE scenario, there are several updates in the ECLIPSE V5a dataset in cement production, transport and introduction of the 12th Five Year Plan for China, compared with the previous versions. Further details please see the IIASA website https://iiasa.ac.at/web/home/research/researchPrograms/air/ECLIPSEv5a.html. The two scenarios span a greater range of aerosol emission uncertainty than the Representative Concentration Pathways (RCPs) used in the 5th Coupled Model Intercomparison Project (CMIP5), or the Shared Socioeconomic Pathways (SSPs) used in CMIP6 (Eyring *et al* 2016). We address two main questions: (1) relative to present day, what are the changes in temperature extremes in near-term future under the two scenarios ? (2) Considering the difference between CLE and MTFR, what are the effects of future AA reductions on temperature extremes, and what are the key physical processes involved in this response?

2. Model and experiments

We use the Met Office Unified Model (Global Coupled configuration 2) HadGEM3-GC2 (Williams *et al* 2015, Wilcox *et al* 2019), with a horizontal resolution of N216. The details of the model are listed in Text S1. The experiments include: a historical experiment forced by GHG concentrations and AA emissions following CMIP5 historical forcings from 1981 to 2005 and then RCP4.5 to 2014 (hereafter HIS); two near-term projection experiments forced by GHG forcing under RCP4.5 scenarios from 2015 to 2049, but performed with different AA future scenarios from the ECLIPSE V5a global emission fields (table S1 is available online at stacks.iop.org/ERL/15/034013/mmedia). The CLE experiment is based on the current legislation AA emission scenario that assumes the implementation of all presently decided emission-related legislation. MTFR employs the maximum technically feasible reduction scenario that assumes full implementation by 2030 of the most advanced technology presently available to drastically reduce aerosol emissions. Emissions of AA and their precursors remain steady in CLE, but are reduced rapidly
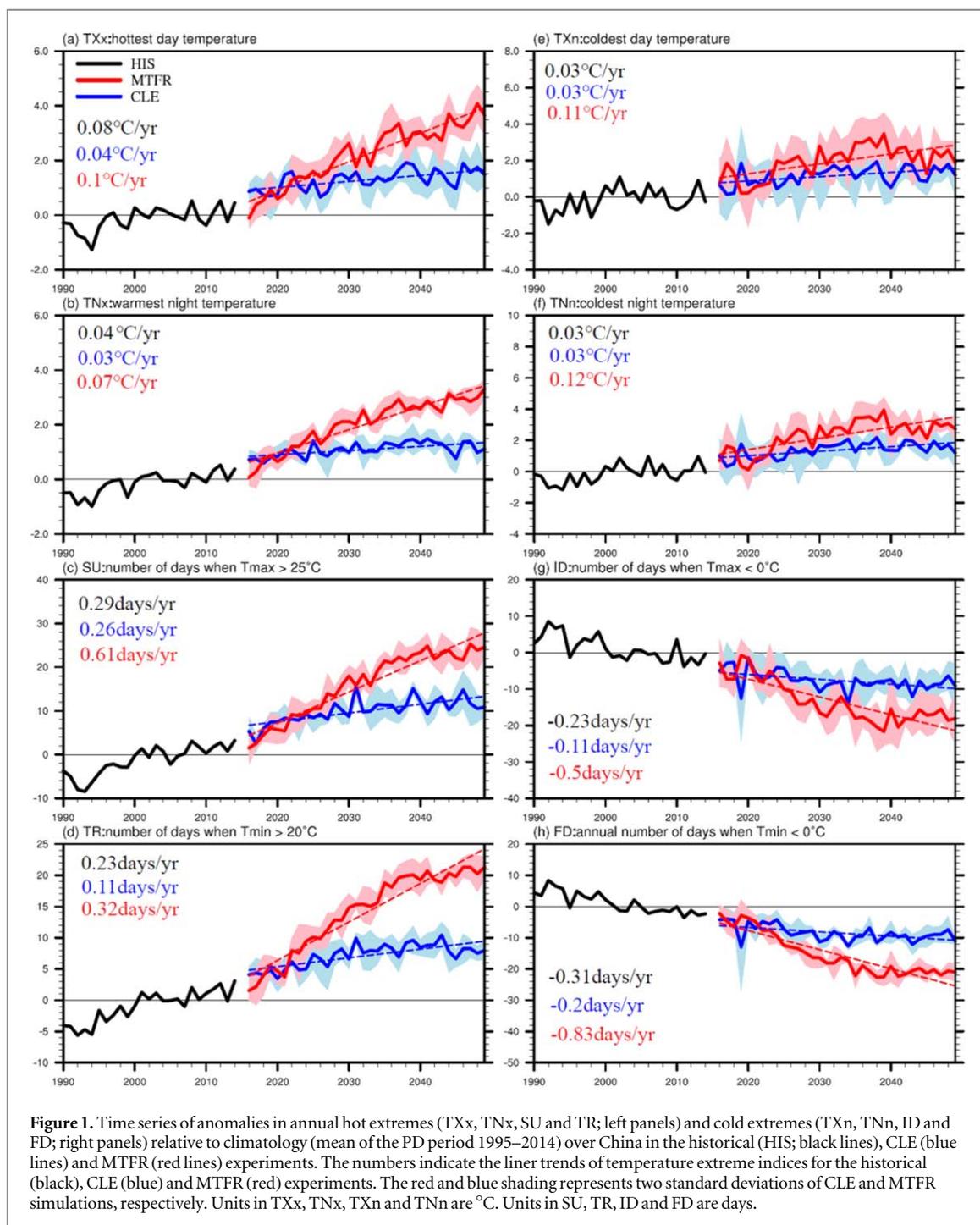
in MTFR, with particularly large reductions over east and south Asia (figure S1). Global AA emissions in CLE hold stably at around $50 \, \text{Tg} \, \text{yr}^{-1}$ during 2016–2049. Emissions in MTFR rapidly drop from 74 to 9.53 Tg from 2016 to 2030, and maintain steady thereafter (figure S1(a)). Relative to the present day (PD: 1995–2014), the global averaged emissions in the near-term future (2016–2049) increase by 3.5% in CLE with Asian emissions increased while European and North American emissions decreased (figure S1(b)), but decrease by 52% in MTFR with global emissions decreased (figure S1(c)).

Each experiment consists of four members that initialize from different atmosphere and ocean states. The ensemble mean of four members for each experiment are analyzed. The mean difference between CLE or MTFR and the historical experiment represents projected changes induced by the combined effect of GHG and AA. The difference between MTFR and CLE denotes the impact of future AA emission reductions.

Our analysis focuses on four hot extreme indices and four cold extreme indices. The hot extreme indices used are: annual hottest daily maximum temperature (TXx); warmest night temperature (TNx); the frequency of summer days (SU, annual number of days when daily maximum temperature (Tmax) $> 25 \, °C$); and tropical nights (TR, annual number of days when daily minimum temperature (Tmin) $> 20 \, °C$). The cold extreme indices used are: annual coldest daily maximum temperature (TXn); coldest night temperature (TNn); the frequency of ice days (ID, annual number of days when Tmax $< 0 \, °C$); and frost days (FD, annual number of days when Tmin $< 0 \, °C$). To evaluate the model's skill in simulating temperature extremes, indices from the historical experiment have been compared with observations from the HadEX2 dataset (Donat *et al* 2013) for 1981–2010. Generally, the model simulates reasonably the spatial variations of the climatological temperature extremes (figures S2–S3; Chen *et al* 2019), and the positive trends in hot extremes, TXn and TNn and negative trends in ID and FD over China and Europe (figures S4–S5; Chen *et al* 2019). This indicates that HadGEM3-GC2 is an appropriate tool for future projections of temperature extremes.

3. Future changes in temperature extremes

Illustrated in figure 1 are the time series of annual temperature extreme indices averaged over mainland China in the three experiments from 1995 to 2049. Relative to HIS, temperature extreme indices are characterized as a rise in TXx, TNx, TXn, TNn, SU and TR, and a decrease in ID and FD under both CLE and MTFR scenarios, indicating changes in both hot extremes and cold extremes over China in the near-term future. This is consistent with the previous understanding (Sillmann *et al* 2013a). All of the time

Figure 1. Time series of anomalies in annual hot extremes (TXx, TNx, SU and TR; left panels) and cold extremes (TXn, TNn, ID and FD; right panels) relative to climatology (mean of the PD period 1995–2014) over China in the historical (HIS; black lines), CLE (blue lines) and MTFR (red lines) experiments. The numbers indicate the liner trends of temperature extreme indices for the historical (black), CLE (blue) and MTFR (red) experiments. The red and blue shading represents two standard deviations of CLE and MTFR simulations, respectively. Units in TXx, TNx, TXn and TNn are °C. Units in SU, TR, ID and FD are days.

series in CLE vary slowly during 2016–2049, with positive trends in the intensity of temperature extremes with a magnitude of around 0.02 °C yr^{-1}, positive trends of 0.2 d yr^{-1} and 0.14 d yr^{-1} for SU and TR, and negative trends of about 0.13 d yr^{-1} for ID and FD, which are slightly smaller or comparable to those in HIS during PD period except TXn (figures 1 and S6(a), (b)). In MTFR magnitudes of the trends are 2–5 times as large as those in the HIS and CLE experiments (figures 1 and S6(a)–(b)), indicating a large sensitivity of trends in temperature extremes to AA pathway. Quantitatively, the area-averaged changes of intensity in temperature extremes between

the near-term future and PD are around 1.2 °C for CLE and 2.0 °C for MTFR, respectively (figures 3(a)). The frequencies of SU and TR increase by 10 (16) days and 7 (14) days for CLE (MTFR), while ID and FD decrease by roughly 8 (14) days for CLE (MTFR), relative to the PD values (figure 3(b)). The uncertainty is represented by 5%–95% confidence intervals in figure 3. For Europe, the changes in temperature extremes in CLE and MTFR are generally similar to those in China in the near-term future relative to PD (figures 2 and S6(c)–(d)), but with the larger area-averaged changes, except for TNx and TR (figures 3(c), (d)).
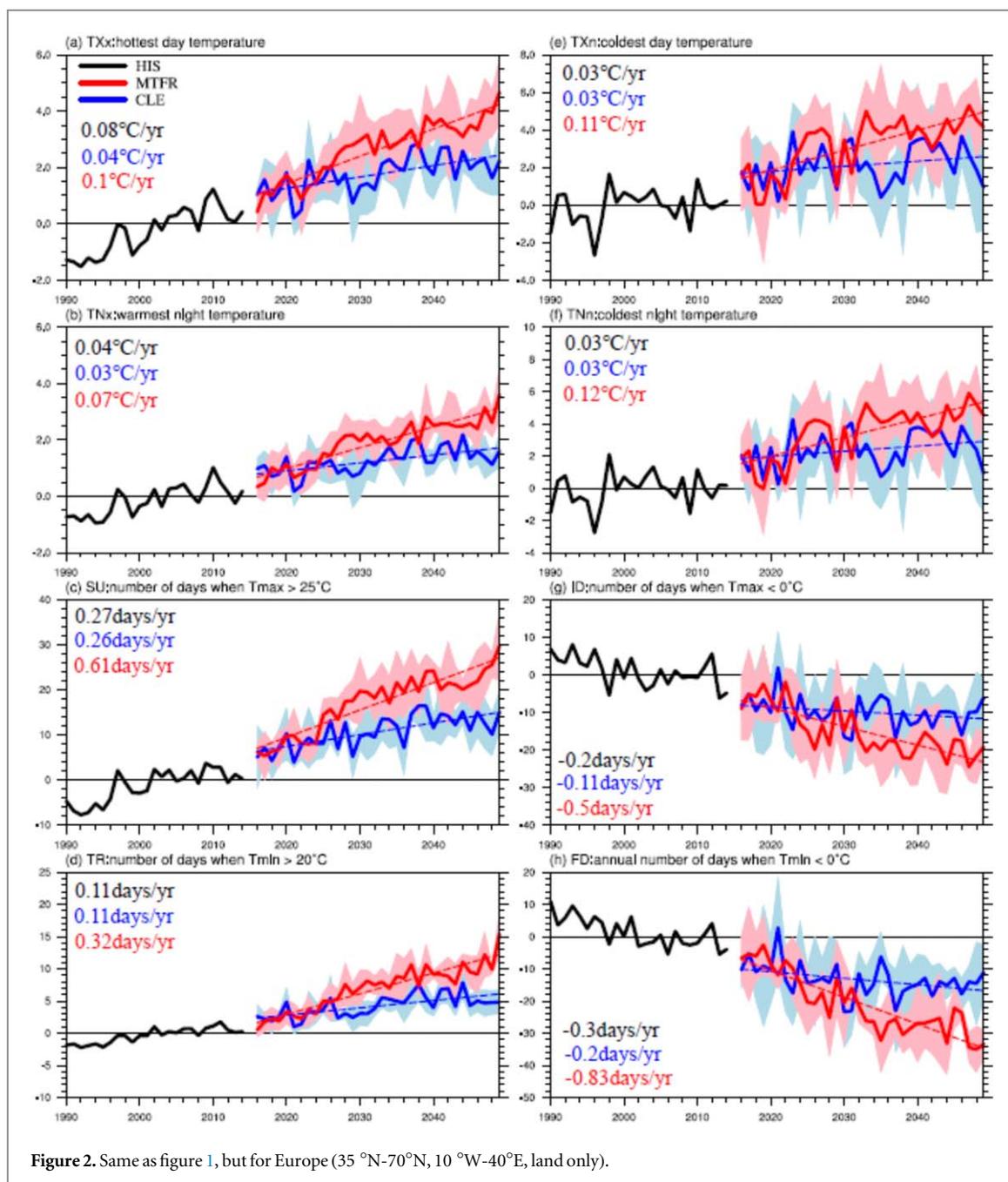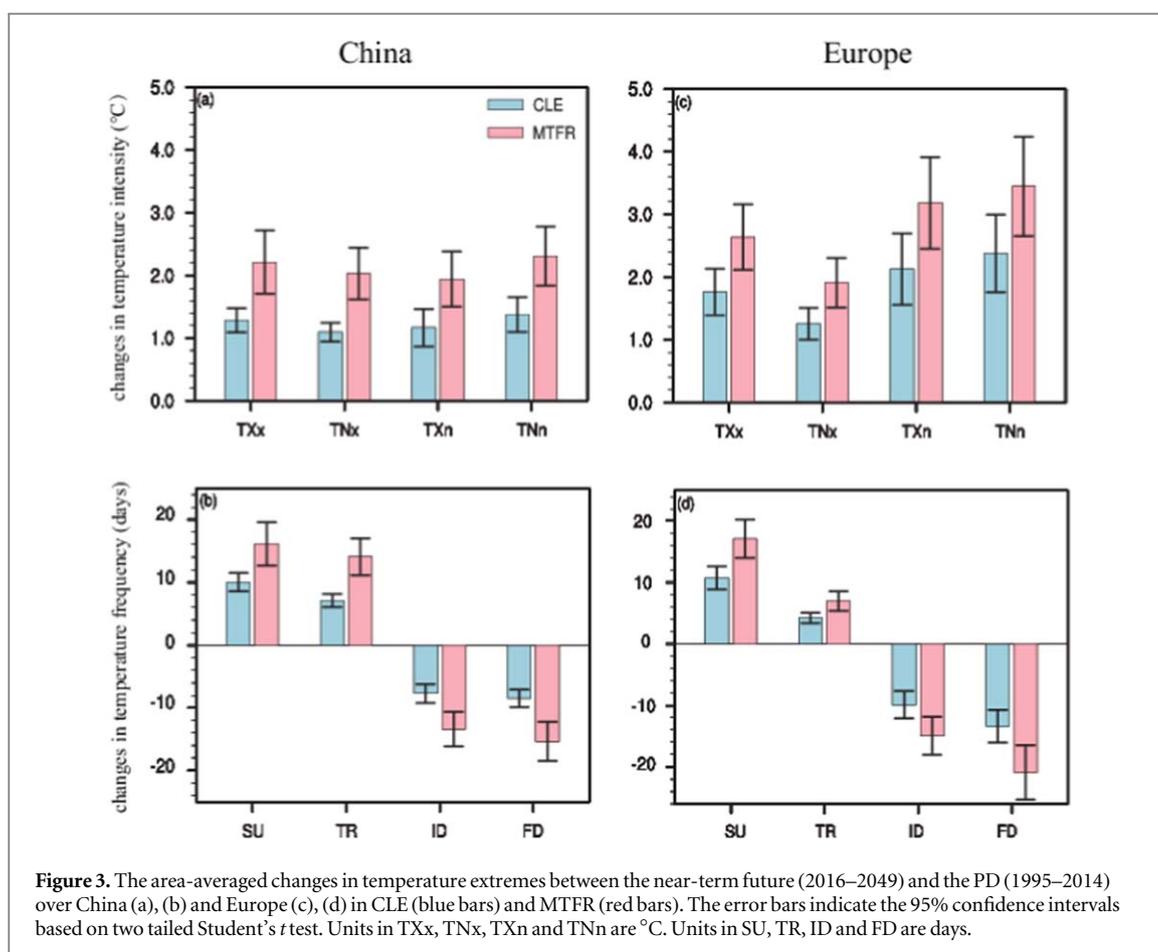
Figure 2. Same as figure 1, but for Europe (35 °N-70°N, 10 °W-40°E, land only).

The main features of future changes are the increase in hot extremes, TXn and TNn, and decrease in ID and FD relative to PD over the Eurasian continent, although the changes show large spatial variations (figures S7–S8). In CLE, the intensity of temperature extremes shows a large increase over eastern Europe, and TXx changes show a relatively large increase over south-eastern China. Additionally, the increase in TXn and TNn is weak and insignificant over most of China except northeastern China and the southern Tibetan Plateau. The changes in SU and TR show an increase, with a large increase over central and southern Europe and central and eastern Europe, respectively. SU and TR changes have a relatively large increase over most of China except over the Tibetan Plateau. Large decreases in ID and FD can be found in eastern Europe and the

Tibetan Plateau. There are similar changes in TNn, TR and FD compared with the previous studies (Sillmann *et al* 2013b, Wang *et al* 2016). However, the significant differences can be seen in TXx. For example, TXx shows a uniform increase over China in Wang *et al* (2016). The maximum increase locates in the Mediterranean region in Sillmann *et al* (2013b), instead of eastern Europe. It should be mentioned that there is no change in hot extreme day over high latitude and in cold extreme day over tropics (figures S7(c), (d) and (g), (h)). This is likely to be a manifestation of a model bias. Since the threshold for these indices is far from the model basic state, the response to anthropogenic forcing is not sufficient to cause a change in the frequencies of variables crossing the thresholds, even though the model simulates trends in absolute temperatures. Such behavior was also

Figure 3. The area-averaged changes in temperature extremes between the near-term future (2016–2049) and the PD (1995–2014) over China (a), (b) and Europe (c), (d) in CLE (blue bars) and MTFR (red bars). The error bars indicate the 95% confidence intervals based on two tailed Student's *t* test. Units in TXx, TNx, TXn and TNn are °C. Units in SU, TR, ID and FD are days.

observed by Chen *et al* (2019). The spatial patterns of the changes in MTFR are similar to those in CLE, but with great magnitude and significant changes.
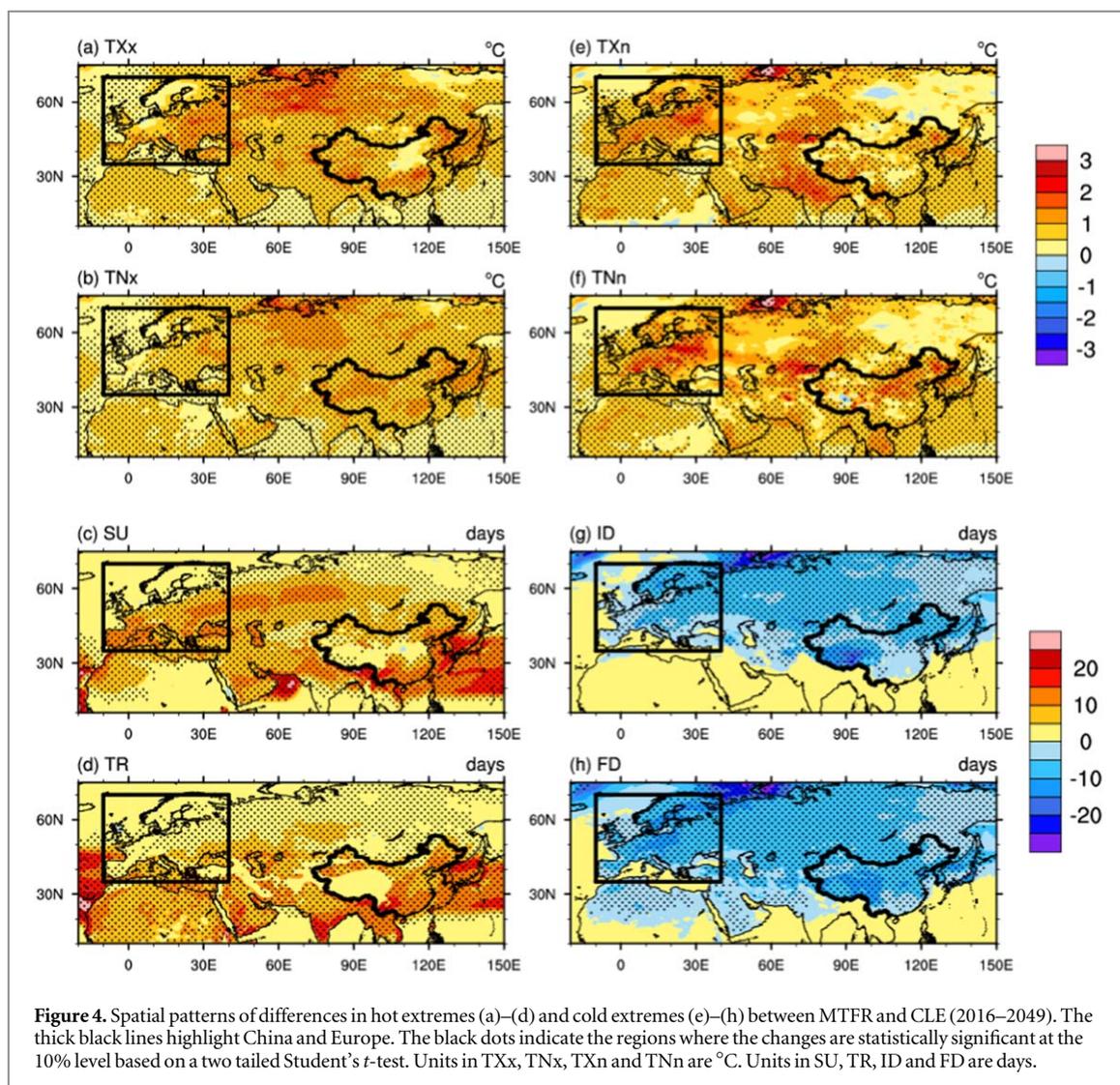
4. Effects of AA reduction

Effects of the global AA reduction are assessed by comparing the changes in MTFR with those in CLE. For China, the most important difference between the two scenarios is that the changes of temperature extremes in MTFR are much faster than those in CLE in the near-term future, showing that magnitudes of the trends in MTFR are 2–5 times as large as those in CLE (figures 1 and S6). Especially, the faster changes in MTFR can be seen during 2016–2030 when rapid emission reductions occur in MTFR, with positive trends of around 0.15 °C yr^{-1} in the intensity, positive (negative) trends of 1.0 (−1.0) d yr^{-1} in the frequency (figure S9). Figure 1 shows that the values of most temperature extreme metrics are significantly different between MTFR and CLE after the 2030 s, except TXn and TNn due to large internal variations in boreal winter, e.g. the significant impacts of the Arctic Oscillation on the cold extremes over East Asia. (Park *et al* 2011; He 2015). These large differences are consistent with the large difference in sulphur dioxide emission between the two scenarios (figure S1(a)). In summary, the AA reduction in MTFR relative to CLE leads to increases in hot

extremes, TXn and TNn and decrease in ID and FD over China in the near-term future.

Quantitatively, the area-averaged difference between MTFR and CLE is around 0.9 °C in TXx and TNx, 6–7 d of SU and TR during 2016–2049 over China (figures 3(a), (b)). MTFR results in 37%~50% larger increases in temperature extremes relative to CLE (figure S10(a)). For cold extremes, the AA reduction leads to an increase of 0.8 °C in TXn and 0.9 °C in TNn, and a decrease of 6–7 d in ID and FD, contributing to approximately 40% of the total changes under MTFR relative to PD (figures 3(a), (b) and S10(a)). All the differences are statistically significant at the 5% level.

For Europe, the effects of reduced AA emissions in MTFR relative to CLE on temperature extremes also induce an increase in hot extremes, TXn and TNn, and a decrease in ID and FD (figure 2). However, there are several overlaps in the time evolution of some metrics between the MTFR and CLE ensembles in this region. These weak separations between the two ensembles are associated with large internal variability in temperature extremes over Europe. Despite this, the area-averaged differences in all metrics are statistically significant at the 5% level (figure 3). The differences show that TXx, TNx, SU and TR increase by 0.9 °C, 0.7 °C, 6 and 3 d, and TXn and TNn increase by about 1.1 °C, and ID and FD decrease by 5 and 8 d (figures 3(c), (d)).

Figure 4. Spatial patterns of differences in hot extremes (a)–(d) and cold extremes (e)–(h) between MTFR and CLE (2016–2049). The thick black lines highlight China and Europe. The black dots indicate the regions where the changes are statistically significant at the 10% level based on a two tailed Student's *t*-test. Units in TXx, TNx, TXn and TNn are °C. Units in SU, TR, ID and FD are days.

The AA reduction explains more than 30% of the total changes under MTFR relative to PD (figure S10(b)). The magnitudes of changes in temperature extremes between MTFR and CLE in Europe are close to those in China (figure 3), although the contribution of the AA reduction to changes in temperature extremes in Europe in the near-term future (2016–2049) relative to PD is slightly smaller than that in China. However, the change in European AA emissions is much smaller than the Asian change (figure S1). This implies that there may be a stronger positive feedback over Europe. Detailed discussion about the positive feedback is in the next section.

Figure 4 displays the spatial patterns of differences in temperature extremes between MTFR and CLE. In general, the effects of AA reductions are that hot extremes, TXn, and TNn increase, and ID and FD decrease over the Eurasian continent, but with large spatial variations. In hot extremes, the differences of TXx and TNx show a local maximum of around 1.5 °C over southeastern China, northeastern China and the Tibetan Plateau. The differences in TXx and TNx also show a local maximum of about 1.5–2 °C and

1–1.5 °C over eastern Europe and the western Siberian plains. There is an insignificant increase in TXx over Scandinavia and North China, with a magnitude of about 0–0.5 °C. The differences in frequency indices show large increases over southern China with about 10–20 d; over western and eastern Europe with 10–15 d for SU; over southern China with 10–20 d; and eastern Europe with 5–10 d for TR. For cold extremes, large increases in TXn and TNn can be seen over central and eastern Europe with a magnitude of about 2–2.5 °C. The TXn and TNn increases are relatively small over most regions in China, except over North China and northeastern China in TNn. The differences in ID show a decrease, with a local maximum of about 20 d over the Tibetan Plateau, and a relatively small decrease over eastern Europe with 5–10 d. The FD decreases show a local maximum of about 10–15 d over the Tibetan Plateau and central Europe. Qualitatively, these changes are in agreement with those in previous study, except the change in TXx over North China (Wang *et al* 2016). It can be found that the regions with maximum changes during the near-term future related to the AA reduction (figure 4) are similar

Figure 5. The area-averaged changes in (a)TXx, TNx, and summer (June–July–August) Tmax and Tmin and (d) TXn, TNn, and winter (December–January–February) Tmax and Tmin between MTFR and CLE (2016–2049) over China (dot bars) and Europe (slashed bars). Spatial patterns of differences in (b), (c) summer and (e), (f) winter Tmax and Tmin between MTFR and CLE. The thick black lines highlight the China and Europe regions. The black dots indicate the regions where the changes are statistically significant at the 10% level based on a two tailed Student's t-test. Units in TXx, TNx, TXn, TNn, Tmax and Tmin are °C.

to changes due to all anthropogenic forcing during the near-term future relative to PD (figures S7–S8), indicating that the AA pathway may play a role in enhancing regional contrasts in changes in temperature extremes in the near-term future, especially over Asia.
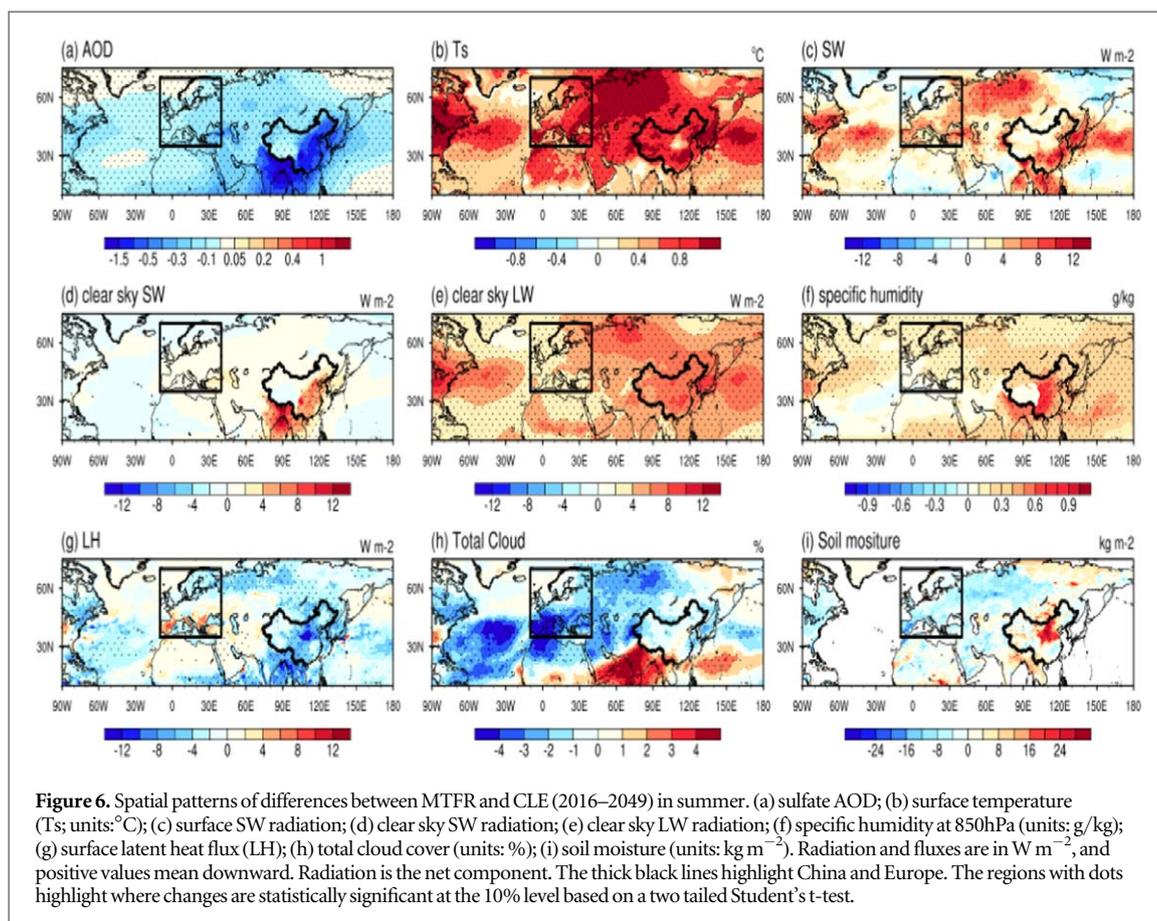
5. Physical processes responsible for the responses to AA reduction

5.1. Seasonal mean surface air temperatures
Figure 5(a) shows a comparison of the area-averaged differences in TXx and TNx with those in the summer seasonal mean Tmax (daily maximum temperature) and Tmin (daily minimum temperature) between MTFR and CLE over China and Europe. The differences in Tmax and Tmin in summer are close to the TXx and TNx changes over China and Europe, suggesting that changes in hot extremes due to reduction in AA over the two regions are predominantly due to the AA induced summer mean Tmax

and Tmin changes. In winter (figure 5(d)), the Tmax and Tmin differences over China are also comparable to the TXn and TNn changes, once again suggesting a dominant role of winter seasonal mean Tmax and Tmin for changes in cold extremes. However, the differences in Tmax and Tmin are nearly half that in TXn and TNn over Europe, suggesting that the changes in cold temperature extremes are partly due to the mean temperature changes and partly due to temperature variability changes. Changes in temperature variability may arise from effects of the North Atlantic Oscillation (NAO) and blocking activities associated with the NAO (e.g. Scaife *et al* 2008, Diao *et al* 2014).

The AA reduction leads to an increase in both Tmax and Tmin over the Eurasian continent. The spatial patterns in Tmax and Tmin changes in summer are similar to those in TXx and TNx changes between MTFR and CLE, such as a large increase over eastern Europe and southeastern China, and a relatively small

Figure 6. Spatial patterns of differences between MTFR and CLE (2016–2049) in summer. (a) sulfate AOD; (b) surface temperature (Ts; units:°C); (c) surface SW radiation; (d) clear sky SW radiation; (e) clear sky LW radiation; (f) specific humidity at 850hPa (units: g/kg); (g) surface latent heat flux (LH); (h) total cloud cover (units: %); (i) soil moisture (units: kg m^{-2}). Radiation and fluxes are in W m^{-2}, and positive values mean downward. Radiation is the net component. The thick black lines highlight China and Europe. The regions with dots highlight where changes are statistically significant at the 10% level based on a two tailed Student's t-test.

increase over northern Europe and North China (figures 4(a), (b) and 5(b), (c)). Similarly, the spatial patterns of Tmax and Tmin changes in winter correspond to those in TXn and TNn changes, which show a large increase over Europe and China and a smaller and insignificant increase over north of the Caspian Sea (figures 4(e), (f) and 5(e), (f)). Hence, the changes of temperature extremes tie in closely with the changes in seasonal mean Tmax and Tmin.
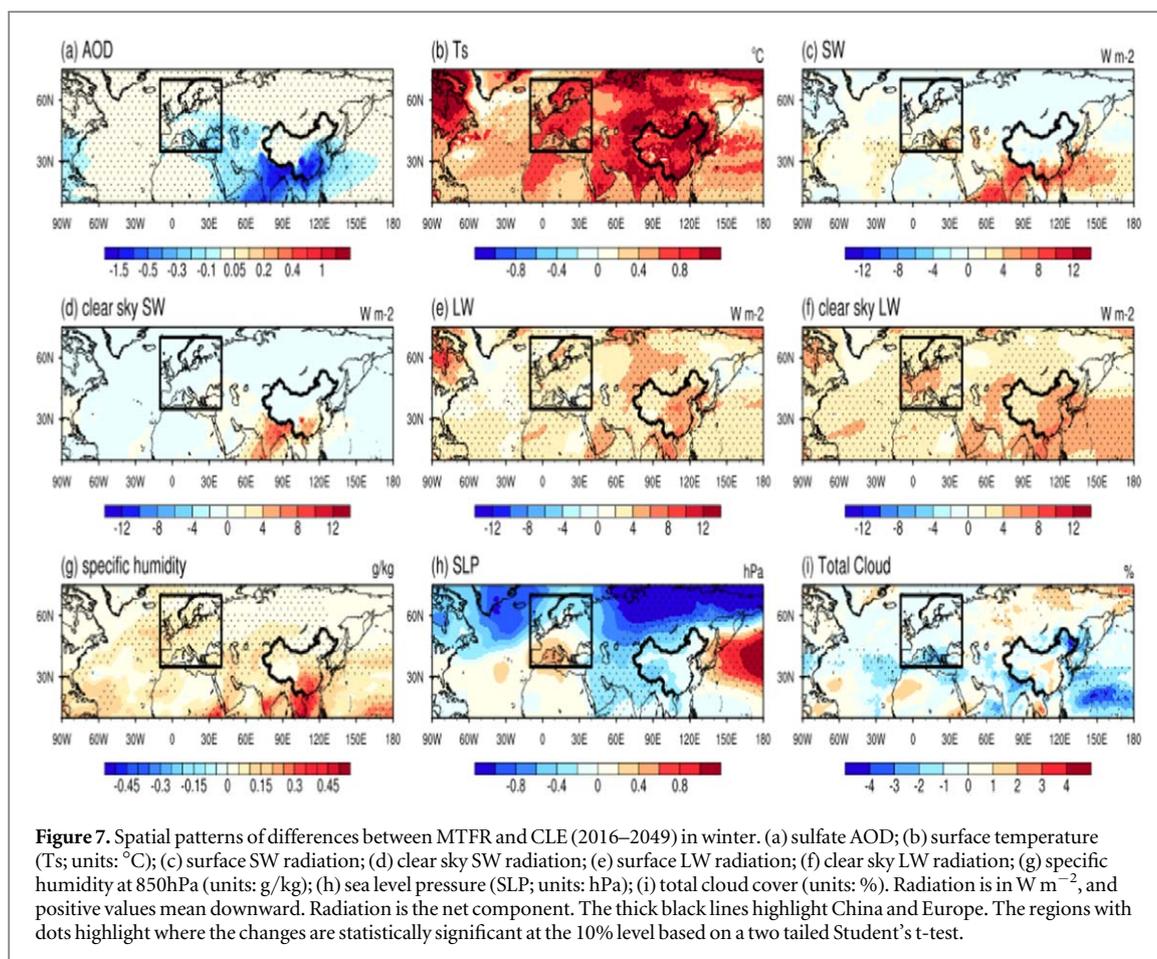
5.2. Physical processes for changes in hot extremes
Figure 6 shows the spatial patterns of summer mean differences for the key components of the surface energy balance and related variables between MTFR and CLE. The difference in sulfate aerosol optical depth (AOD) is characterized by a decrease over Eurasia with a local maximum over East Asia and South Asia (figure 6(a)), which is closely related to the changes in sulfur dioxide emissions (figure S1). Note that changes in AA in the model experiments include differences in both sulfate and carbonaceous aerosol. However, differences in sulfate AOD are much larger than changes in the other species (figure S11), indicating that the responses to AA differences are predominantly due to the changes in sulfur dioxide.

The AA reduction induces significant surface warming over Eurasia (figure 6(b)) through different processes in different regions. There is good correspondence in the

patterns of changes in net surface shortwave (SW) and clear sky longwave (LW) and those in surface warming. In particular, the large increase in surface temperature in northern Eurasia, which is far from the maximum changes in AOD, is related to positive changes in the surface SW (figure 6(c)), which are mainly due to a decrease in total cloud fraction (figure 6(h)), since surface clear sky SW changes are small there (figure 6(d)). In addition, the positive changes in surface clear sky LW, related to increased water vapor in the atmosphere (figures 6(e), (f)), also makes a contribution to surface warming.

The large decreases in AOD over East Asia lead to positive changes in net clear-sky SW (~6 W m^{-2}) over Eastern China via aerosol-radiation interactions (figure 6(d)), which are responsible for the positive changes in net surface SW that warm the land surface. In addition, positive changes in net surface clear-sky LW (4–6 W m^{-2}) warm the land surface over most of China (figures 6(e) and S12(a)), which result from the increased water vapor in the atmosphere (figure 6(f)). This increase in water vapor is likely to be associated with the strengthened East Asian summer monsoon (EASM) with southwesterly and southerly anomalies along the coast of East China through enhanced land sea warming contrast (figures S12(c), (d) and 6(b)). The EASM response to the AA forcing is in agreement with previous results (Tian *et al* 2018, Dong *et al* 2019). Interestingly, there is a relatively weak and

Figure 7. Spatial patterns of differences between MTFR and CLE (2016–2049) in winter. (a) sulfate AOD; (b) surface temperature (Ts; units: °C); (c) surface SW radiation; (d) clear sky SW radiation; (e) surface LW radiation; (f) clear sky LW radiation; (g) specific humidity at 850hPa (units: g/kg); (h) sea level pressure (SLP; units: hPa); (i) total cloud cover (units: %). Radiation is in W m^{-2}, and positive values mean downward. Radiation is the net component. The thick black lines highlight China and Europe. The regions with dots highlight where the changes are statistically significant at the 10% level based on a two tailed Student's t-test.

insignificant warming over North China (figure 6(b)), which is reflected in the changes in TXx and summer Tmax (figures 4(a) and 5(b)). This could be due to the enhanced EASM, which leads to increased soil moisture over North China and the enhanced upward latent heat flux (LH) (~ -8 W m^{-2}) there (figures 6(g) and (i)).

For Europe, the surface warming mainly results from positive change in net surface SW with a magnitude of 4~6 W m^{-2}, due to positive changes in shortwave cloud radiative effect (SW CRE) (i.e. the difference between net SW and net clear sky SW) (figures 6(c), (d)). These positive SW CRE changes are associated with reduced cloud cover (figure 6(h)) that partially results from aerosol-cloud interactions related to reduced AA emissions and partially results from reduced soil moisture (figure 6(i)), indicating a positive feedback between the land and atmosphere over Europe (Dong *et al* 2016a). The deficit of soil moisture leads to an increased upward sensible heat fluxes (figure S12(c)), which could give rise to drier and warmer air and enhance evaporative demand, which dries the soil further. Decreased soil moisture leads to decreased upward latent heat flux (figure 6(g)), especially over southern Europe. This loop could lead to further reductions in cloud fraction and to further positive changes in surface SW. An increase in water vapor from the North Atlantic due to warm SST

anomalies there and a strengthened North Atlantic summer jet (figures 6(f) and S12(d)) induces the increase of net clear sky LW (4~8 W m^{-2}), which also contributes to surface warming over Europe (figures 6(b), (e), (f)).

5.3. Physical processes for changes in cold extremes

The AA reduction causes significant warming over Eurasia in winter (figure 7(b)), mainly through positive changes in clear sky LW (figure 7(f)) with an additional contribution from positive SW changes over southern Europe (figure 7(c)). Positive changes in clear sky LW are associated with increased water vapor in the atmosphere (figure 7(g)). The increase in water vapor should be related to a positive NAO-like pattern that leads to warm maritime air to Eurasia (figure 7(h)). In winter, the changes in AOD are smaller over Europe, resulting in weak changes in local downwelling SW (figure 7(d)). Over China, the largest decrease in AOD is in the southeast, which causes an increase in downwelling shortwave (figures 7(c), (d)). This contributes to the warming, alongside the positive change in LW due to the increase in atmospheric water vapor (figures 7(f), (g)). Additionally, there is a big warming in northern Eurasia, which is partly due to positive changes in clear sky LW, related to increase in the water vapor in the atmosphere, and partly due to

positive changes in LW CRE, related to the increase in cloud cover (figures 7(e)–(i)).

6. Conclusion and discussion

In this study, we have investigated the changes in temperature extremes over China and Europe in the near-term future (2016–2049) relative to the present day (1995–2014). We have estimated the effects of potential future rapid reductions in anthropogenic aerosols by performing a set of experiments using HadGEM3-GC2 with two very different AA emission scenarios: aerosol and precursor emissions expected if current legislation remains in force (CLE), and the reductions expected if all currently technically feasible methods were put in place (MTFR).

Relative to the present day, the hot extremes (TXx, TNx, SU, and TR) averaged over China during 2016–2049 increase under both the CLE and MTFR scenarios. For the cold extremes, TXn and TNn averaged over China increase, and ID and FD decrease, under both scenarios, representing a decreasing intensity and frequency of cold extremes. The large aerosol reductions in MTFR result in greater projected changes relative to present day: about 40% larger compared to CLE. All the changes in the temperature extremes over China are statistically significant at the 5% level under the MTFR scenario. Changes of a similar magnitude are seen over Europe although significance is smaller due to larger internal variability. The aerosol reductions in MTFR result in an enhancement of future warming relative to CLE of over 30%.

The changes of temperature extremes are determined mainly by changes in seasonal mean surface air temperatures (Tmax and Tmin). The global AA reduction leads to a decrease in AOD over Eurasia with a maximum over East Asia, which tends to warm the surface. During summer, the surface warming is caused by the positive changes in net clear-sky SW via aerosol-radiation interaction over China, with an additional contribution from water vapor feedback. The warming over Europe is mainly due to the positive changes in SW CRE, that partially results from aerosol-cloud interactions related to reduced AA emissions and partially results from positive atmosphere-land feedbacks. During winter, positive changes in net clear-sky LW at the surface are an important factor for the surface warming over Eurasia and arise due to an increase in water vapor in the atmosphere due to warm SST anomalies over the western Pacific and North Atlantic. However, changes in surface SW are weak, and they are not the main factors for winter warming over Eurasia.

The results in this study agree qualitatively with those in previous studies, indicating that a global AA reduction will greatly enhance the effect of GHG forcing and lead to more hot extremes and less cold extremes in the near-term future (Sillmann *et al* 2013b, Wang *et al* 2016). Moreover, our experimental design samples a larger range of future aerosol uncertainty than the RCPs used in CMIP5. As such, our results suggest a much stronger effect (∼40%) on the temperature extremes over China than that (∼24%) under RCP8.5 scenario in Wang *et al* (2016). Hence, because of the policy dependence of AA emissions and model-related uncertainties, the effect of AA reductions on climate extremes requires further study under different scenarios and in additional models. Additionally, recent studies have suggested that the snow darkening effect may play an important role in altering regional climate, such as warmer Eurasian continent in summer (e.g. Sang *et al* 2019). Hence, without accounting for aerosol effects on snow albedo in the model may lead to biases in surface temperature simulations. However, the results would not be expected to change greatly, considering a dominate role of sulfate in this study. Consequently, concomitant with the AA reduction due to air quality measures, faster GHG reduction should be considered to mitigate global warming in future emission control strategies.

Acknowledgments

Data availability statement

The data that support the findings of this study are available from the corresponding author upon reasonable request.

ORCID iDs

Feifei Luo ⓘ https://orcid.org/0000-0003-3587-5547
Buwen Dong ⓘ https://orcid.org/0000-0003-0809-7911
Qin Su ⓘ https://orcid.org/0000-0001-9707-5153
Wei Chen ⓘ https://orcid.org/0000-0003-3161-8447

References

Acosta Navarro J *et al* 2017 Future response of temperature and precipitation to reduced aerosol emissions as compared with increased greenhouse gas concentrations *J. Clim.* **30** 939–54

Alexander V *et al* 2006 Global observed changes in daily climate extremes of temperature and precipitation *J. Geophys. Res. Atmos.* **111** D05109

Chen W and Dong B 2018 Anthropogenic impacts on recent decadal change in temperature extremes over China: relative roles of

greenhouse gases and anthropogenic aerosols *Clim. Dyn.* **52** 3643–60

Chen W *et al* 2019 Attribution of recent trends in temperature extremes over China: role of changes in anthropogenic aerosol emissions over Asia *J. Clim.* **32** 7539–60

Diao Y, Xie S and Luo D 2014 Asymmetry of winter European surface air temperature extremes and the North Atlantic Oscillation *J. Clim.* **28** 517–30

Donat G *et al* 2013 Updated analyses of temperature and precipitation extreme indices since the beginning of the twentieth century: the HadEX2 dataset *J. Geophys. Res. Atmos.* **118** 1–16

Dong B, Sutton R and Shaffrey L 2016a Understanding the rapid summer warming and changes in temperature extremes since the mid-1990s over Western Europe *Clim. Dyn.* **48** 1537–54

Dong B *et al* 2016b Abrupt summer warming and changes in temperature extremes over Northeast Asia since the mid-1990s: drivers and physical processes *Adv. Atmos. Sci.* **33** 1005–23

Dong B, Wilcox L, Highwood E and Sutton R 2019 Impacts of recent decadal changes in Asian aerosols on the East Asian summer monsoon: roles of aerosol–radiation and aerosol–cloud interactions *Clim. Dyn.* **53** 3235–56

Eyring V, Bony S, Meehl G A, Senior C A, Stevens B, Stouffer R J and Taylor K E 2016 Overview of the coupled model intercomparison project phase 6 (CMIP6) experimental design and organization *Geosci. Model Dev.* **9** 1937–58

Fischer E and Knutti R 2015 Anthropogenic contribution to global occurrence of heavy-precipitation and high-temperature extremes *Nat. Clim. Change* **5** 560–4

He S 2015 Asymmetry in the Arctic oscillation teleconnection with January cold extremes in Northeast China *Atmos. Oceanic Sci. Lett.* **8** 386–91

Hienola A *et al* 2018 The impact of aerosol emissions on the 1.5 °C pathways *Environ. Res. Lett.* **13** 044011

Mickley L *et al* 2012 Regional warming from aerosol removal over the United States: results from a transient 2010–2050 climate simulation *Atmos. Environ.* **46** 545–53

Park T, Ho C and Yang S 2011 Relationship between the Arctic Oscillation and cold surges over East Asia *J. Clim.* **24** 68–83

Samset B *et al* 2018 Climate impacts from a removal of anthropogenic aerosol emissions *Geophys. Res. Lett.* **45** 1020–9

Sang J *et al* 2019 Possible impacts of snow darkening effects on the hydrological cycle over western Eurasia and East Asia *Atmosphere* **10** 500

Scaife A *et al* 2008 European climate extremes and the North Atlantic Oscillation *J. Clim.* **21** 72–83

Sillmann J *et al* 2013a Climate extremes indices in the CMIP5 multimodel ensemble: II. Future climate projections *J. Geophys. Res. Atmos.* **118** 2473–93

Sillmann J *et al* 2013b Aerosol effect on climate extremes in Europe under different future scenarios *Geophys. Res. Lett.* **40** 2290–5

Sun Y *et al* 2014 Rapid increase in the risk of extreme summer heat in Eastern China *Nat. Clim. Change* **4** 1082–5

Tebaldi C *et al* 2006 Going to extremes: an intercomparison of model-simulated historical and future changes in extreme events *Clim. Change* **79** 185–211

Tian F *et al* 2018 Forced decadal changes in the East Asian summer monsoon: the roles of greenhouse gases and anthropogenic aerosols *Clim. Dyn.* **51** 3699–715

Wang Z *et al* 2016 The effect of future reduction in aerosol emissions on climate extremes in China *Clim. Dyn.* **47** 2885–99

Wilcox L *et al* 2018 Multiple perspectives on the attribution of the extreme European summer of 2012 to climate change *Clim. Dyn.* **50** 3537–55

Wilcox L *et al* 2019 Mechanisms for a remote response to Asian aerosol emissions in boreal winter *Atmos. Chem. Phys.* **19** 9081–95

Williams D *et al* 2015 The Met office global coupled model 2.0 (GC2) configuration *Geosci. Model Dev.* **8** 1509–24

Wuebbles D *et al* 2014 CMIP5 climate model analyses: climate extremes in the United States *Bull. Amer. Meteor. Soc.* **95** 571–83

Xu J *et al* 2013 Projected changes in climate extremes over China in the 21st century from a high resolution regional climate model (RegCM3) *Chin. Sci. Bull.* **58** 1443–52

Xu Y *et al* 2018 Projected changes in temperature and precipitation extremes over China as measured by 50 yr return values and periods based on a CMIP5 ensemble *Adv. Atmos. Sci.* **35** 376–88

Zhou B *et al* 2014 Projected changes in temperature and precipitation extremes in China by the CMIP5 multimodel ensembles *J. Clim.* **27** 6591–611